ARTICLE

https://doi.org/10.1038/s41586-018-0184-1

Observation of half-integer thermal Hall conductance

Mitali Banerjee[1], Moty Heiblum[1]*, Vladimir Umansky[1], Dima E. Feldman[2], Yuval Oreg[1] & Ady Stern[1]

Topological states of matter are characterized by topological invariants, which are physical quantities whose values are quantized and do not depend on the details of the system (such as its shape, size and impurities). Of these quantities, the easiest to probe is the electrical Hall conductance, and fractional values (in units of e^2/h, where e is the electronic charge and h is the Planck constant) of this quantity attest to topologically ordered states, which carry quasiparticles with fractional charge and anyonic statistics. Another topological invariant is the thermal Hall conductance, which is harder to measure. For the quantized thermal Hall conductance, a fractional value in units of κ_0 ($\kappa_0 = \pi^2 k_B^2/(3h)$, where k_B is the Boltzmann constant) proves that the state of matter is non-Abelian. Such non-Abelian states lead to ground-state degeneracy and perform topological unitary transformations when braided, which can be useful for topological quantum computation. Here we report measurements of the thermal Hall conductance of several quantum Hall states in the first excited Landau level and find that the thermal Hall conductance of the 5/2 state is compatible with a half-integer value of $2.5\kappa_0$, demonstrating its non-Abelian nature.

The even-denominator fractional quantum Hall state in the first excited Landau level at a bulk filling factor of $\nu = 5/2$ has been a subject of extensive research for the past thirty years[1]. After its first observation[2], it was suggested that this state might be a manifestation of superconducting-like condensation of composite fermions in a zero effective magnetic field[3–5]. Furthermore, it was predicted that the state carries quasiparticles whose mutual exchange statistics is non-Abelian[3]. Consequently, the ground state of several quasiparticles remains degenerate even at their fixed positions; hence, such states are attractive for topological quantum computing[1]. Yet, this prediction has been hard to test experimentally because relatively easily accessible experimental probes, such as electric response functions, do not reflect the topological order of the state. Even after the demonstration of the state's quasiparticle charge[6,7] being $e^* = e/4$ and the observation of a topologically protected upstream-propagating neutral mode[8], a family of possible orders are still viable candidates for the $\nu = 5/2$ state. However, the thermal Hall conductance may distinguish Abelian from non-Abelian states because it is quantized to an integer value of $\kappa_0 T$, where T is the temperature, for the former and a half-integer value for the latter[5]. Furthermore, its precise value distinguishes between different candidate orders. Here, we report an observation compatible with such half-integer quantization.

Background

It is worth giving a brief summary of the different orders predicted for this state. Numerical work lent support[9–11] to the non-Abelian Pfaffian[3] and anti-Pfaffian topological orders[12,13]. Among the other possible states are the $SU(2)_2$, the $K = 8$, 331 and 113 liquids, as well as their particle–hole conjugates[14–17]. A non-Abelian particle–hole Pfaffian order[13,18–21] with the wave function described in ref. [19] was interpreted in terms of Dirac composite fermions[18]. Although the naming of these states does not follow any particular methodology, a wire construction organizes them in terms of their thermal Hall conductance, introduces possible generalizations, for which the thermal Hall conductance may be any arbitrary integer or half-integer multiple[22] of $\kappa_0 T$, and identifies their edge structure (see below). Our goal is to determine the experimentally relevant order from thermal transport.

The thermal Hall conductance is defined in a two-terminal measurement as $g_Q = dJ_Q/dT = KT$, with J_Q being the heat current (in watts) and K the thermal conductance coefficient. This highly important characteristic of the system has a maximal value for one-dimensional ballistic channels, with $K = \kappa_0$. The thermal Hall conductance is independent of the charge and the exchange statistics of the heat-carrying particles. This quantum limit has been experimentally realized for bosons[23,24], fermions[25] and recently for a strongly interacting system—the lowest Landau level in the fractional quantum Hall effect (with fractionally charged quasiparticles)[26]. In the latter study[26] it was shown that in the presence of counter-propagating one-dimensional modes and in the limit of a long propagation length, the thermal conductance reflects the net number of topological chiral modes (the number of downstream modes minus the number of upstream modes), as predicted by the K matrix in the bulk[27].

Among the possible topological orders for the $\nu = 5/2$ state[16], the non-Abelian candidates are predicted to conduct $n + 1/2$ ($n = 0, 1, \ldots, 4$) units of the quantized heat, J_Q, whereas for Abelian states the 1/2 is missing. The term 1/2 originates from a neutral edge mode (it can be downstream or upstream) whose central charge is one-half. This mode may be viewed as a Majorana chiral edge mode of a superconductor of composite fermions. Moreover, each of the proposed non-Abelian topological orders has a different n, implying a different fractional quantized thermal conductance, g_Q. Hence, measuring the heat conductance of the equilibrated $\nu = 5/2$ fractional state may determine the nature of the topological order. Our measurement results are compatible with $K \approx 2.5\kappa_0$.

Experimental details

Our experimental setup, with its 'heart' shown in Fig. 1a, is similar in principle to our previously studied configuration[26] (see Methods). The two-dimensional electron gas is structured in the form of four separated arms (formed by chemical etching), with a small floating reservoir

[1]Braun Center of Sub-Micron Physics, Department of Condensed Matter Physics, Weizmann Institute of Science, Rehovot, Israel. [2]Department of Physics, Brown University, Providence, RI, USA.
*e-mail: moty.heiblum@weizmann.ac.il

© 2018 Macmillan Publishers Limited, part of Springer Nature. All rights reserved.

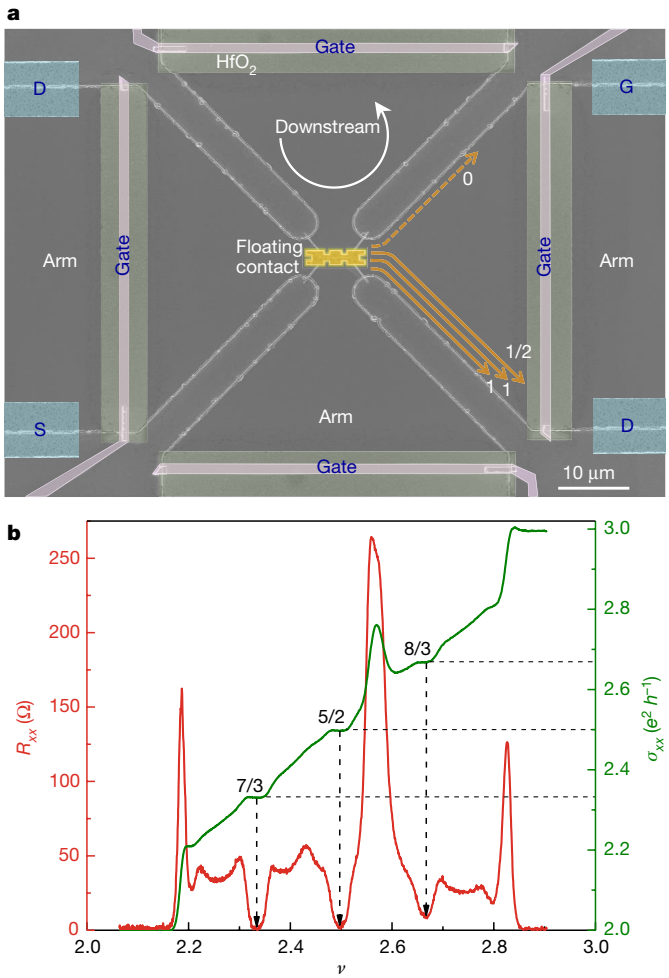

Fig. 1 | Device configuration and Hall data. a, The 'heart' of the device. For a description of the whole structure, see ref. [26]. The small ohmic contact (with an area of 12 μm^2) serves as the heated floating reservoir, injecting currents into N arms. The effective propagation length (to a cold contact) in each arm is about 150 μm. The thermal noise can be measured in two opposite arms (connected to band-pass filters and cold amplifiers). Arms can be disconnected by negatively charging surface gates deposited on HfO_2. Although the voltage required to disconnect an arm by a typical quantum point contact is about −10 V, which leads to severe hysteresis and instability, only about −1 V sufficed with the surface gates. This allowed stable operation. As an example, the energy-carrying edge modes that correspond to the particle–hole Pfaffian order are shown. The solid orange arrows represent downstream charge modes; each carries a heat flux of $\kappa_0 T$. The dashed orange arrow represents an upstream Majorana mode carrying a heat flux of $0.5\kappa_0 T$. S, source; D, drain; G, gate. **b**, The longitudinal resistance, R_{xx}, and the transverse Hall conductance, σ_{xx}, in the first excited Landau level, measured in a separate Hall bar (length, 200 μm; width, 100 μm) fabricated with the same MBE-grown material as that used in the experiment.

in the centre (an ohmic contact with an area of about 12 μm^2) heated by an incident direct current to temperature T_m. The chiral edge modes leave the floating reservoir and enter the separated arms with temperature T_m. Each arm is gated across its width with a continuous metallic surface gate (isolated from the sample's surface by 5-nm-thick HfO_2), about 30 μm away from the floating reservoir. Negative charging of each gate allows disconnecting the corresponding arm from the circuit.

If I_s is the source current, then the incident current at the floating reservoir is $I_{in} = t_1 I_s$, where $t_1 = \nu_{gate}/\nu$ is the transmission coefficient of the source's arm gate, ν_{gate} is the filling factor under the gate. The outgoing current splits into N arms, with the dissipated power in the floating reservoir being $\Delta P = P_{in} - P_{out} = 0.5 I_{in} V_s (1 - N^{-1})$, where V_s is the Hall voltage, with all gates uncharged. In thermal equilibrium, the dissipated power equals—ideally—the outgoing power carried by the chiral one-dimensional charged edge modes and by the phonons (to the bulk); namely, $\Delta P = \Delta P_e + \Delta P_{ph}$. The edge modes are expected to carry a heat of $\Delta P_e = (1/2) n_{tot} K (T_m^2 - T_0^2)$, where $n_{tot}K$ is the overall thermal conductance coefficient of n_{tot} modes in N arms, and T_0 is the electron temperature in the grounded contacts. In turn, the heat flux carried by phonons is expected to obey[28] $\Delta P_{ph} = \beta (T_m^5 - T_0^5)$.

The temperature T_m was determined by measuring the thermal noise (in the downstream drain) carried by the current leaving the floating reservoir. We emphasize that owing to the chirality of the modes (and the absence of back-scattering), the low-frequency current fluctuations leaving the floating reservoir are conserved. Thus, the downstream thermal current fluctuations reflect the temperature of the floating contact (even if the edge modes cool along their paths). The voltage fluctuations in the drain, S_v (in V^2 Hz^{-1}) were filtered by an LC circuit located at the mixing chamber (with frequency $f_0 \approx 695$ kHz and bandwidth $\Delta f = 30$ kHz). The relevant thermal current fluctuations S_{th} were calculated via $S_{th} = S_v G_H^2$, where $G_H = \nu e^2/h$. The voltage fluctuations were amplified by a cascade of a 'cold' (at 4.2 K) and a room-temperature amplifier and measured by a spectrum analyser. In our setup, the voltage gain of the cold amplifier, calibrated via thermal and shot-noise measurements (normalized to a bandwidth of 30 kHz), was about 9, with an input-referred noise of 260 pV Hz$^{-1/2}$. The gain of the room-temperature amplifier was 200, with an input-referred noise of 0.5 nV Hz$^{-1/2}$.

Following the procedure described in ref. [26] (see Methods), the temperature T_m was plotted as a function of the dissipated power, ΔP. Additional contributions to the thermal conductance (for example, from phonons and bulk electrons) that depend only on T_m, were subtracted (hereafter referred to as 'subtraction procedure'); namely, $\delta P_{\Delta N} = \Delta P(N_i, T_m) - \Delta P(N_j, T_m)$, where $i > j$, with $N_k = 2, 3, 4$ being the total number of open arms. This procedure allows a direct determination of the change of the heat flow due to changes in the number of conducting arms. Following this analysis, we plot a normalized coefficient for $\Delta N = N_i - N_j$ open arms, $\lambda_{\Delta N}/\Delta N = \delta P_{\Delta N}/(\kappa_0/2)$, as a function of T_m^2, with the slope being the normalized thermal conductance, K/κ_0, of a single arm (or a single mode). To strengthen our conclusions we also show selected data of (1) the total heat transport of N_k open arms, which contains also heat flux that is not associated with the chiral edge modes and (2) data analysis that includes the phonon contribution.

The molecular beam epitaxy (MBE)-grown GaAs–AlGaAs heterostructures that hosted the two-dimensional electron gas were designed to screen effectively the ionized dopants (Extended Data Fig. 1). Consequently, 'relatively free' electrons that reside in the doping regions can contribute to the electrical and thermal conductance. We carried out initial experiments with an extremely high-mobility two-dimensional electron gas by employing short-period superlattice doping (SPSL), with excess electrons in the doping layer[29]. The low-temperature dark mobility was 31×10^6 cm^2 V^{-1} s^{-1} and the areal electron density was 3.1×10^{11} cm^{-2}. Clear Hall plateaus and a longitudinal resistance of $R_{xx} < 10$ Ω were observed for filling factors of $\nu = 2$–3 (Extended Data Fig. 2). Although the electrons in the doping layer were relatively localized (owing to their heavy mass and the disorder), they still seemed to conduct heat. For example, when testing the heat flow at $\nu = 2$, where the thermal conductance is well understood, we found it to be higher than the expected value by approximately $3\kappa_0 T$. The subtraction procedure led to the expected heat conductance in each arm (Extended Data Fig. 3); yet, the accuracy required in these experiments necessitated a minimization of such unwanted contributions.

Consequently, we developed a 'delta-doped' scheme in a low-Al-mole-fraction $Al_xGa_{1-x}As$ layer ($x \approx 0.23$–0.25). This led to shallower silicon deep-donor-like levels[30]. As in the SPSL scheme, excess doping was required to obtain good conductance quantization in states with $\nu = 2$–3. The shallower donor level allowed a relatively low 'freezing temperature' of the electrons and thus a still efficient screening of the donors. However, sufficient charge localization was

© 2018 Macmillan Publishers Limited, part of Springer Nature. All rights reserved.

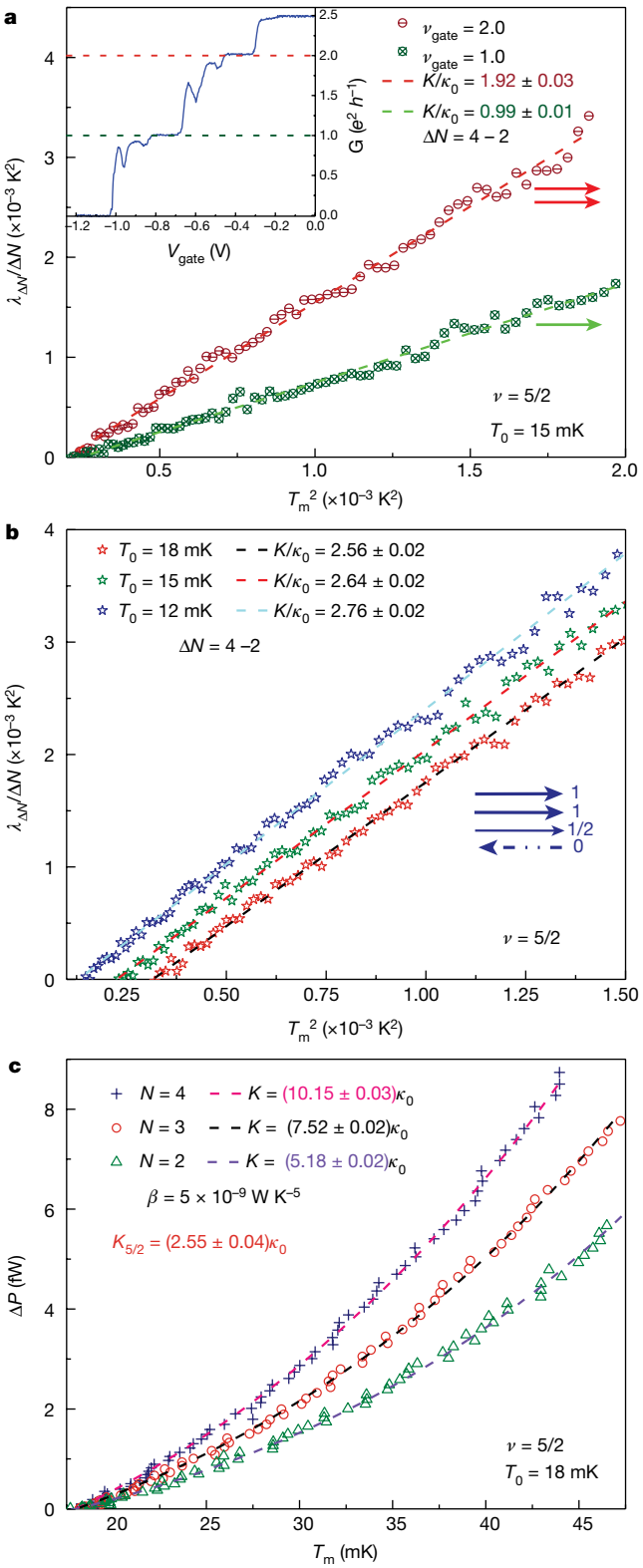

Fig. 2 | Heat flow of the two outermost edge modes at bulk filling $\nu = 5/2$. a, The normalized heat flow $\lambda_{\Delta N}/\Delta N = \delta P_{\Delta N}/(\kappa_0/2)$, with δP being the difference in heat dissipation between $N = 4$ (four open arms) and $N = 2$ (two arms are open), with $\Delta N = 2$, as a function of T_m^2. Two different realizations were studied: two downstream edge modes per arm (two red arrows, $\nu_{gate} = 2$) and one downstream edge mode per arm (one green arrow, $\nu_{gate} = 1$). The slopes of the fitted lines represent the normalized heat conductance, $K/\kappa_0 \approx 1.92$ for $\nu_{gate} = 2$ and $K/\kappa_0 \approx 0.99$ for $\nu_{gate} = 1$. The errors in the slopes are regressive errors (in the least-squares fitting procedure). The inset shows the transmission of a typical arm gate as a function of the gate voltage, with two plateaus that correspond to two or one edge modes propagating in the arm. **b**, Similar measurements with four and two arms fully transmitting (zero or slightly positive gate voltage). Measurements were performed at three different base electron temperatures, T_0, with K/κ_0 increasing at lower temperatures. The arrows describe an idealized edge-mode structure of the particle–hole Pfaffian order as in Fig. 1a. **c**, Total power dissipation with $N = 4$, 3 and 2, plotted as a function of T_m for $T_0 = 18$ mK. K is determined by fitting the data with the expression $\Delta P = 0.5NK(T_m^2 - T_0^2) + \beta(T_m^5 - T_0^5)$ for the established phonon coefficient, β (see text). An average $K = 2.54\kappa_0$ is found. All of the errors mentioned here are confidence levels of between 95% and 99%.

achieved at base temperature, with negligible bulk heat conductance. We conducted measurements in a sample with a dark mobility of about 20×10^6 cm^2 V^{-1} s^{-1} and areal electron density 2.8×10^{11} cm^{-2}, with a smaller span of the quantized Hall plateaus in a magnetic field and a higher lowest R_{xx} (Fig. 1b).

The sample was cycled three times between room temperature and low temperatures. This cycling process is known to change the distribution of charged impurities and donors, effectively rendering a slightly different device microscopically. Measurements were repeated at different temperatures and different magnetic fields (in particular, at different fillings on the $\nu = 5/2$ plateau). Deducing the thermal conductance with a reasonable accuracy necessitates a careful determination of the parameters of the system. The following important factors were considered in the measurements (see also Methods). (i) Source noise. A non-ideal source contact may produce noise, which in turn will add to the measured thermal noise. Being uncorrelated with the thermal noise, if small enough, this noise is easily subtracted from the measured thermal noise. (ii) Equal division of currents and the overlap of Hall plateaus among the different arms (Extended Data Fig. 4). Although in general the uniformity of the electron density was excellent and the contact resistance was isotropic, small adjustments were done, when needed, by changing slightly the magnetic field. (iii) Because the small floating contact does not have zero contact resistance, incident (or emitted) currents may suffer reflection. Reflection was found to depend on the base temperature, the cycling round and the filling factor. In general, the reflection coefficient was found to be always smaller than 3%, with no remarkable difference between the thermal conductance determined in different runs. (iv) The stability of the electron base temperature, T_0, during the long measurements of the thermal noise is crucial. Hence, consecutive measurements at different temperatures were performed after long intervals that allowed the electrons to reach a constant temperature. (v) An accurate determination of the amplification in the different Hall states under study is crucial. The amplification did not change considerably among the nearby $\nu = 7/3$, 5/2 and 8/3 states studied (see Methods). (vi) Systematic errors resulted mostly from the uncertainty (±0.5 mK) in determining the electrons' temperature, which is directly tied to accuracy in determining the correct amplifier gain. We estimated the total error in the determination of the thermal conductance coefficient (due to regression and systematic errors) to be less than $\pm 0.05\kappa_0$ at a confidence level of more than 90%. Interestingly, the correct determination of T_0 led to an excellent linear-dependence fit of the power dissipation with T_m^2 (at low enough temperatures, where phonon contribution is negligible, or by employing the subtraction procedure) for any number N of open arms. (vii) During the measurements, the electrons initially remained at temperatures of around 18–20 mK (with a fridge temperature of about 10 mK) and later slowly cooled to 11–12 mK (with a fridge temperature <6 mK). Measurements at higher temperatures necessitated heating up the fridge.

Measurement results

We start by presenting the measurements performed at a bulk filling factor of $\nu = 5/2$. To verify the integrity of our measurements (for example, the amplification and the electron temperature), we first

© 2018 Macmillan Publishers Limited, part of Springer Nature. All rights reserved.

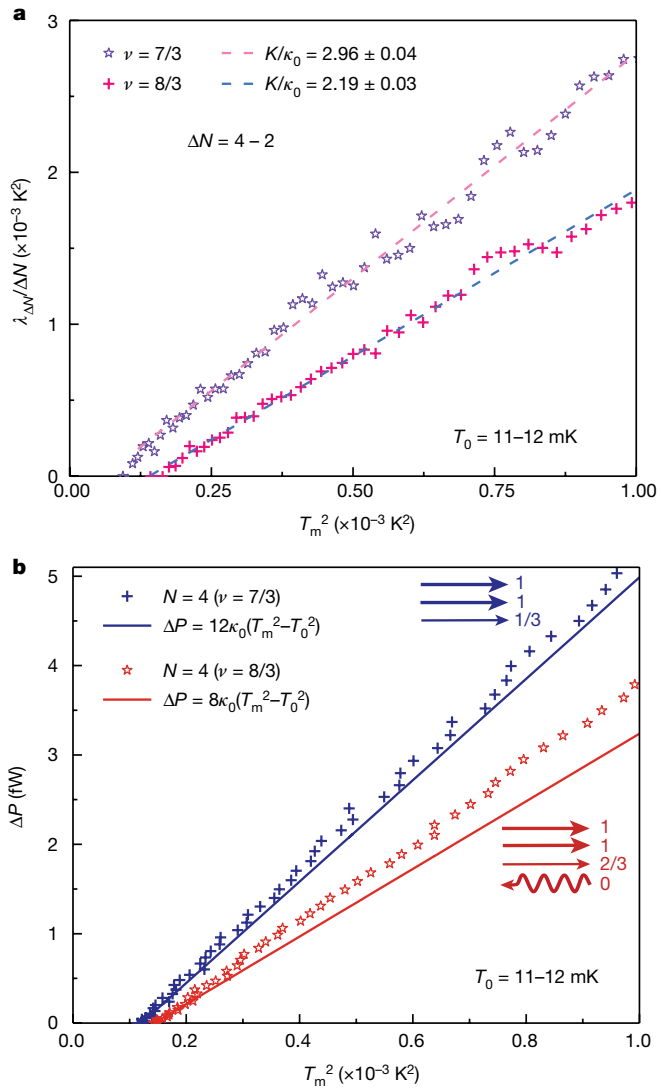

Fig. 3 | Normalized heat conductance at bulk fillings $\nu = 7/3$ and $\nu = 8/3$. a, A similar measurement to that shown in Fig. 2a for the two neighbouring fractional states to $\nu = 5/2$. For the $\nu = 7/3$ state $K_{7/3} = (2.96 \pm 0.05)\kappa_0$, with average $K_1 = (0.99 \pm 0.03)\kappa_0$ for a single edge mode. In the $\nu = 8/3$ state (errors mentioned are at a confidence level of better than 95%), with an upstream propagating neutral mode, $K = 2\kappa_0$ is expected for an infinite propagation length. The observed thermal conductance coefficient is larger (similar to that of the $\nu = 2/3$ state[26]). **b**, The total dissipated power is plotted for the two states in **a** as a function of T_m^2 (without any data manipulation). Arrows describe the edge structure of each of the states. The measured power dissipation at $\nu = 7/3$ agrees well with the expected one, with a weak deviation at higher temperatures (likely due to the phonon contribution). In the $\nu = 8/3$ state the deviation is greater owing to the lack of equilibration, combined with bulk heat conductance due to the finite R_{xx}.

measured the heat conductance of the two outmost integer edge modes. As verified previously[25,26], the thermal conductance is expected to be an integer multiple of $\kappa_0 T$. By tuning the voltage of the arm gates (Fig. 1a), thus controlling the fillings under the gates, to either $\nu_{gate} = 1$ or $\nu_{gate} = 2$, the outermost-edge mode or the two outer-edge modes, respectively, were allowed to reach the remote grounds (inset, Fig. 2a). Under these conditions, the inner modes of the fractional $\nu = 1/2$ state were fully reflected back into the floating contact. Measurements were performed with $N = 4$, 3 and 2, and here we plot the normalized electronic power dissipation of a single arm, $\lambda_{\Delta N}/\Delta N$ for $\Delta N = 2$, as a function of T_m^2 (following the subtraction procedure). The slope of each curve corresponds to the corresponding normalized heat conductance coefficient, K/κ_0 (Fig. 2a). For $\nu_{gate} = 2$, the heat conductance for the two modes is $K_2 = (1.92 \pm 0.05)\kappa_0$, whereas for $\nu_{gate} = 1$ we find $K_1 = (0.99 \pm 0.04)\kappa_0$, with an average heat conductance per mode of $K_1 = (0.97 \pm 0.03)\kappa_0$. The small deviations from the expected values emanate from systematic and random errors (see above), as well as from possible non-ideality of the system. Yet, the results reproduce recent measurements of integer modes in altogether different devices[26].

In Fig. 2b we present the most important results of this work measured at the $\nu = 5/2$ state. With the gates unbiased, the heat was carried away from the floating reservoir into each open arm. Because this state may harbour counter-propagating modes, downstream charge modes and upstream neutral modes, a complete equilibration of the modes within each arm's edge is necessary to correctly determine the order of the $\nu = 5/2$ state. Hence, a propagation length substantially longer than the equilibration length (which is expected to decrease as the temperature increases[26]) is required (here, $L \approx 150$ μm). A length that is too short may also harbour non-topological counter-propagating edge modes due to undesirable edge reconstruction. However, bulk contribution may have an important role for long arms because it may induce thermal flux backflow. We start by analysing the data with the subtraction procedure, which is applied to the data from the centre of the conductance plateau at three different base electron temperatures, T_0. By plotting the normalized electronic power dissipation of a single arm, $\lambda_{\Delta N}/\Delta N$ for $\Delta N = 2$, as a function of T_m^2, we observe a linear dependence at the three base temperatures of the electrons (confirming the correct determination of the temperature). As the temperature decreases, an increase in the heat conductance is evident, which we attribute to an increase of the temperature equilibration length. At higher temperatures, the thermal conductance tends to saturate with $K_{5/2} = (2.53 \pm 0.04)\kappa_0$, whereas at the lowest temperature we find $K_{5/2} = (2.76 \pm 0.04)\kappa_0$; we address this observation in more detail later.

To validate our measurement results, we present also raw data in Fig. 2c (and Fig. 3). In the plot, the total power dissipation ΔP at $T_0 = 18$ mK is shown as a function of T_m for different numbers of arms. We find $K_{5/2} = (2.55 \pm 0.04)\kappa_0$ for a single, fully open arm. The dashed lines are least-squares fits using $K(T_m^2 - T_0^2) + \beta(T_m^5 - T_0^5)$, with $\beta = 5 \times 10^{-9}$ W K^{-5}, where K is a single free parameter used to fit the data points. Fixing a single β (which depends on the size of our floating contact) as above leads to an uncertainty in K of ~$0.02\kappa_0$ in the present analysis; this agrees with the uncertainty in the subtraction procedure. As can be seen in the figures, the fits across the full temperature range are in excellent agreement with the data points, as the chosen β provides the lowest accumulated error in the fitting line (in all our datasets).

We then studied the two neighbouring fractional states, the simpler $\nu = 7/3$ state and the $\nu = 8/3$ hole-conjugate state. The $\nu = 7/3$ state is expected to support only three downstream charge modes: two integer and one fractional (the inner $\nu = 1/3$, $e^* = e/3$)[31], each with central charge[26] equal to 1. The hole-conjugate $\nu = 8/3$ state, similarly to the $\nu = 2/3$ state in the lowest Landau level, also supports three downstream charge modes, two integer and one fractional (the inner $\nu = 2/3$, with $e^* = e/3$)[31], but the inner mode is accompanied by an upstream neutral mode (with central charge equal to 1). Effectively, in fully equilibrated transport, a net of two modes carries the heat[26].

Representative results in the above two states, obtained using the subtraction procedure at $T_0 = 11$–12 mK, are shown in Fig. 3b (see also Extended Data Fig. 5). In Fig. 3a, for $T_m(\max) \approx 30$ mK, $\nu = 7/3$ and for a fully open arm we find the thermal conductance coefficient to be $K_{7/3} = (2.96 \pm 0.04)\kappa_0$. This corresponds to an average of $K_1 = (0.99 \pm 0.03)\kappa_0$ per single charge edge mode (integer or fractional). For the $\nu = 8/3$ state, we find a thermal conductance coefficient of $K_{8/3} = (2.19 \pm 0.03)\kappa_0$ instead of the expected $K_{8/3} = 2\kappa_0$ for fully equilibrated counter-propagating modes. We note also the finite R_{xx} at $\nu = 8/3$ (larger than in the other two neighbouring states; see Fig. 1b), which may lead to heat leakage into the bulk, thus effectively increasing the apparent thermal conductance. It is important to recall that in previous measurements of the heat conductance at the fractional $\nu = 2/3$ state we found $K_{2/3} = 0.33\kappa_0$ at $T_0 = 10$ mK and $K_{2/3} = 0.25\kappa_0$ at

© 2018 Macmillan Publishers Limited, part of Springer Nature. All rights reserved.

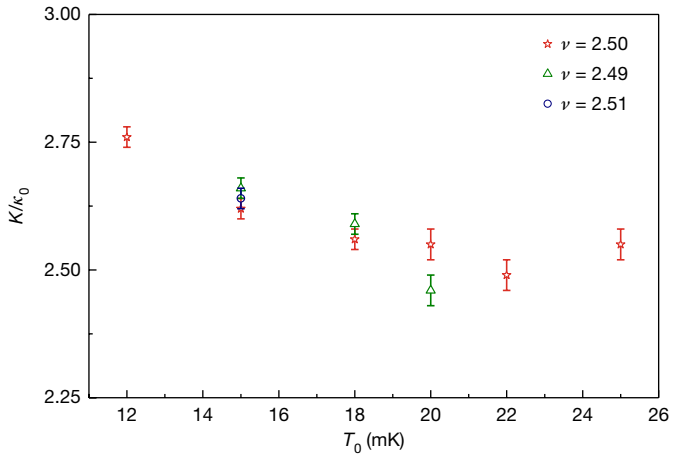

Fig. 4 | Summary of the normalized thermal conductance coefficient results for $\nu = 5/2$. Plotted is the average K/κ_0 as a function of the temperature at three different fillings on the $\nu = 5/2$ G_H conductance plateau. A clear tendency of increased thermal conductance at lower temperatures is visible. Such dependence is attributed to the increased equilibration length (among downstream and upstream modes) at lower temperatures (see ref. [26] for a similar behaviour of the $\nu = 2/3$ state). Seventeen measurements were conducted, with K/κ_0 falling in the range $K/\kappa_0 = (2.53 \pm 0.04)\kappa_0$ at electron base temperatures of $T_0 = 18$–25 mK, where most of the data points were taken.

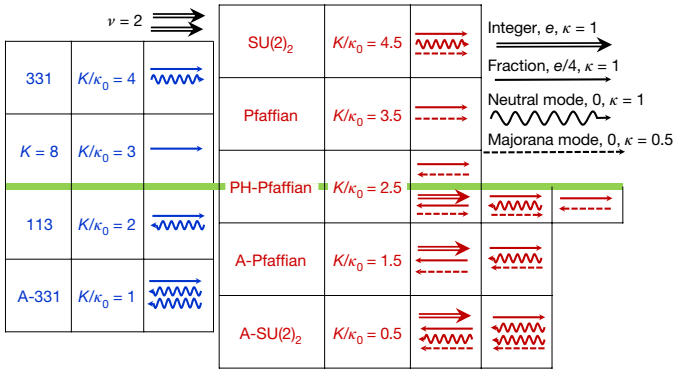

Fig. 5 | Possible orders predicted for the $\nu = 5/2$ state. Edge-mode structure of the leading candidates for the many-body state of a fractional quantum Hall $\nu = 5/2$ liquid: Pfaffian, anti-Pfaffian (A-Pfaffian) and particle–hole Pfaffian (PH-Pfaffian) topological orders and the SU(2)$_2$, $K = 8$, 331 and 113 liquids ('A' stands for 'anti'). Their expected quantized thermal Hall conductance, KT, in units of $\kappa_0 T$ are also shown. A right-pointing double-line arrow denotes a downstream edge mode of a fermion with charge $e^* = e$, contributing Hall conductivity $G_H = e^2/h$ and $K/\kappa_0 = 1$. Right- and left-pointing solid-line arrows denote a downstream and an upstream fractional charge mode, respectively, contributing $0.5G_H = e^2/(2h)$ and $K/\kappa_0 = 1$. The wavy line denotes a fermionic neutral mode with zero charge and $K/\kappa_0 = 1$, and the dashed line denotes a Majorana mode with zero charge and $K/\kappa_0 = 1/2$. A neutral mode with $K/\kappa_0 = 1$ is physically equivalent to two Majorana modes. The left (right) part of the figure depicts the Abelian (non-Abelian) states with an integer (half-integer) K/κ_0. For all states, the lowest Landau level is fully occupied, as shown by the two downstream fermions (the two black right-pointing double-line arrows in the top left part of the figure). The $\nu = 5/2$ state can be constructed in a particle-like manner, starting from $\nu = 2$ and adding fractional, neutral, or Majorana modes, or in a hole-like fashion, starting from $\nu = 3$ and adding modes moving in opposite directions (for example, see the third column of the anti-Pfaffian phase). The final state of the edge modes, after full equilibration, is depicted in the right-most column of each row. The green line divides the particle-like and hole-like states.

$T_0 = 30$ mK. Such dependence on the temperature is expected because it is tied directly with the temperature dependence of the equilibration length (see methods in ref. [26]). The presence of neutral modes in $\nu = 8/3$ and in $\nu = 5/2$ was also verified (see Extended Data Fig. 6).

In Fig. 3 we show raw data for the two neighbouring states near $\nu = 5/2$ without any data manipulation (such as the subtraction procedure or taking into account the phonon contribution). The total heat dissipation for $N = 4$ is plotted in Fig. 3b as a function of T_m^2. For the $\nu = 7/3$ state, a deviation from $K_1 = \kappa_0$ for a single charge mode (namely, $K_{7/3} = 3\kappa_0$ in each arm) becomes evident when the temperature approaches about 30 mK, which is clearly due to the phonon contribution. Yet, for the $\nu = 8/3$ state, the deviation from the expected total thermal conductance of $8\kappa_0$ (for four arms) is more apparent. Here, the non-equilibrated heat transport, combined with additional bulk transport (because $R_{xx} > 0$), contributes to a larger deviation of the thermal conductance.

In Fig. 4 we summarize the normalized thermal conductance coefficient of the $\nu = 5/2$ state. We plot K/κ_0 at different temperatures (12–25 mK) and at three filling factors (on the $\nu = 5/2$ conductance plateau). Seventeen measurements were performed with the device temperature cycled three times to room temperature, thus allowing for different microscopic configurations of the ionized charges. A saturation of the normalized thermal conductance $K_{5/2} = (2.53 \pm 0.04)\kappa_0$ is observed in the temperature range $T_0 = 18$–25 mK. The thermal conductance increases when the temperature is ≤ 15 mK. Such dependence is attributed to the increased equilibration length among the counter-propagating modes at lower temperatures (see the next section and Methods). In Fig. 5 we have summarized some of the more likely edge structures of possible orders that may describe the $\nu = 5/2$ state, as well as their equilibrated K/κ_0 values.

Discussion and conclusions

Composite fermions and the K-matrix formalism provide a powerful framework for the understanding of the fractional quantum Hall effect in the lowest Landau level. Almost all the quantum Hall states in the lowest Landau level are believed to be integer quantum Hall liquids of composite fermions[32]. Our recent results on thermal transport in the lowest Landau level strongly support that picture[26]. The first excited Landau level poses a greater challenge. The nature of the $\nu = 5/2$ and $\nu = 12/5$ states has long been a puzzle. Competing proposals have also been made for the $\nu = 7/3$ and $\nu = 8/3$ states[33,34]; however, past[31,35] and present results prove that these two states are compatible with composite fermion liquids, similar to those at $\nu = 1/3$ and $\nu = 2/3$.

We now discuss our measurement results and their implications. In this study and in our previous work[26], the results agree well with theoretical predictions[36], with a level of precision of about 1% (in sufficiently long samples). Two of the states require further elaboration. For the $\nu = 2/3$ state, theory predicts a thermal Hall conductance that scales like $1/L$ (with L being the system size), with a proportionality constant that decreases with temperature (see methods in ref. [26]). Our measurements are compatible with this expectation. For the $\nu = 8/3$ state, we observed a thermal Hall conductance exceeding the expected one by about 10%, which we also attribute to partial equilibration of counter-propagating edge modes and the finite R_{xx} of this state. When examining the case of $\nu = 5/2$, these results give confidence in our experimental setup and analysis.

For the $\nu = 5/2$ state, taking our findings of $K_{5/2} = 2.5\kappa_0$ at face value, the results are compatible with the topological order of the particle–hole Pfaffian liquid[18,19]. On the basis of common theoretical understanding, the fractional value of K implies that the $\nu = 5/2$ state is non-Abelian. The identification of this topological order is rather surprising, in view of the numerical works that predicted the Pfaffian and anti-Pfaffian topological orders as leading candidates. This discrepancy may be reconciled by models that include disorder[37–39].

There may be factors that would cause the measured thermal Hall conductance to be different from that imposed by the bulk topological order. Of these, we note the lack of equilibration of counter-propagating edge modes and leakage of heat to the bulk either due to longitudinal electronic thermal conductance or due to phonons. We were able to quantify the phonons' contribution and ascertain that it is small

© 2018 Macmillan Publishers Limited, part of Springer Nature. All rights reserved.

(otherwise, we fully subtracted it). The observation of plateau-like saturation in the measured two-terminal thermal conductance suggests that the contribution of the longitudinal conductance is small, although the level of precision of the plateau cannot rule out that such contribution exists.

To analyse possible effects of partial equilibration, we consider an edge carrying upstream modes with a thermal Hall conductance coefficient K_u and downstream modes with a thermal Hall conductance coefficient K_d. Full equilibration at the edge, which is expected for long enough samples, would result in a measured thermal Hall conductance coefficient of $|K_d - K_u|$, whereas in the absence of any equilibration the measured thermal Hall conductance coefficient would be $K_d + K_u$. Partial equilibration may give rise to intermediate values between these two limits. If some of the modes on an edge fully equilibrate while others stay intact, a plateau will arise with a heat conductance that is different from that dictated by the topological order in the bulk (with a possible distribution of the heat current between the two edges of the sample). Remarkably, the difference between the values of the heat conductance in the two models is an integer. Thus, an observed half-integer value in this case implies that the topological order is non-Abelian. In particular, such a picture (with equilibration of only certain modes) might be consistent with the anti-Pfaffian topological order[40]. Hence, although our results point at the $\nu = 5/2$ state being non-Abelian, they might not fully identify its topological order.

Online content

Any Methods, including any statements of data availability and Nature Research reporting summaries, along with any additional references and Source Data files, are available in the online version of the paper at https://doi.org/10.1038/s41586-018-0184-1.

Received: 30 September 2017; Accepted: 26 March 2018;
Published online 4 June 2018.

1. Nayak, C. et al. Non-Abelian anyons and topological quantum computation. *Rev. Mod. Phys.* **80**, 1083–1159 (2008).
2. Willett, R. et al. Observation of an even-denominator quantum number in the fractional quantum Hall effect. *Phys. Rev. Lett.* **59**, 1776–1779 (1987).
3. Moore, G. et al. Nonabelions in the fractional quantum Hall effect. *Nucl. Phys. B* **360**, 362–396 (1991).
4. Greiter, M. et al. Paired Hall state at half filling. *Phys. Rev. Lett.* **66**, 3205–3208 (1991).
5. Read, N. et al. Paired states of fermions in two dimensions with breaking of parity and time-reversal symmetries and the fractional quantum Hall effect. *Phys. Rev. B* **61**, 10267–10297 (2000).
6. Dolev, M. et al. Observation of quarter of an electron charge at the $\nu = 5/2$ quantum Hall state. *Nature* **452**, 829–834 (2008).
7. Radu, I. P. et al. Quasi-particle properties from tunneling in the $\nu = 5/2$ fractional quantum Hall state. *Science* **320**, 899–902 (2008).
8. Bid, A. et al. Observation of neutral modes in the fractional quantum Hall regime. *Nature* **466**, 585–590 (2010).
9. Morf, R. H. Transition from quantum Hall to compressible states in the second Landau level: new light on the $\nu = 5/2$ enigma. *Phys. Rev. Lett.* **80**, 1505–1508 (1998).
10. Storni, M. et al. Fractional quantum Hall state at $\nu = 5/2$ and the Moore–Read Pfaffian. *Phys. Rev. Lett.* **104**, 076803 (2010).
11. Rezayi, E. H. Landau level mixing and the ground state of the $\nu = 5/2$ quantum Hall effect. *Phys. Rev. Lett.* **119**, 026801 (2017).
12. Levin, M. et al. Particle-hole symmetry and the Pfaffian state. *Phys. Rev. Lett.* **99**, 236806 (2007).
13. Lee, S. S. et al. Particle–hole symmetry and the $\nu = 5/2$ quantum Hall state. *Phys. Rev. Lett.* **99**, 236807 (2007).
14. Wen, X. G. Non-Abelian statistics in the fractional quantum Hall states. *Phys. Rev. Lett.* **66**, 802–805 (1991).
15. Halperin, B. I. Theory of the quantized Hall conductance. *Helv. Phys. Acta* **56**, 75–102 (1983).
16. Yang, G. et al. Influence of device geometry on tunneling in $\nu = 5/2$ quantum Hall liquid. *Phys. Rev. B* **88**, 085317 (2013).
17. Yang, G. *et al*. Experimental constraints and a possible quantum Hall state at $\nu = 5/2$. *Phys. Rev. B* **90**, 161306 (2014).
18. Son, D. T. Is the composite fermion a Dirac particle? *Phys. Rev. X* **5**, 031027 (2015).
19. Zucker, P. T. et al. Stabilization of the particle–hole Pfaffian order by Landau-level mixing and impurities that break particle–hole symmetry. *Phys. Rev. Lett.* **117**, 096802 (2016).
20. Fidkowski, L. et al. Non-Abelian topological order on the surface of a 3D topological superconductor from an exactly solved model. *Phys. Rev. X* **3**, 041016 (2013).
21. Bonderson, P. et al. A time-reversal invariant topological phase at the surface of a 3D topological insulator. *J. Stat. Mech.* **2013**, P09016 (2013).
22. Kane, C. L. et al. Pairing in Luttinger liquids and quantum Hall states. *Phys. Rev. X* **7**, 031009 (2017).
23. Schwab, K. et al. Measurement of the quantum of thermal conductance. *Nature* **404**, 974–977 (2000).
24. Meschke, M. et al. Single-mode heat conduction by photons. *Nature* **444**, 187–190 (2006).
25. Jezouin, S. et al. Quantum limit of heat flow across a single electronic channel. *Science* **342**, 601–604 (2013).
26. Banerjee, M. et al. Observed quantization of anionic heat flow. *Nature* **545**, 75–79 (2017).
27. Wen, X. G. *Quantum Field Theory of Many-body Systems: From the Origin of Sound to an Origin of Light and Electrons* (Oxford Univ. Press, Oxford, 2004).
28. Wellstood, F. C. et al. Hot-electron effects in metals. *Phys. Rev. B* **49**, 5942–5955 (1994).
29. Umansky, V. et al. in *Molecular Beam Epitaxy: From Research to Mass Production* (ed. Henini, M.) 121–137 (Elsevier, Amsterdam, 2013).
30. Mooney, P. M. Deep donor levels (DX centers) in III–V semiconductors. *J. Appl. Phys.* **67**, R1–R26 (1990).
31. Dolev, M. et al. Characterizing neutral modes of fractional states in the second Landau level. *Phys. Rev. Lett.* **107**, 036805 (2011).
32. Jain, J. K. *Composite Fermions* (Cambridge Univ. Press, Cambridge, 2007).
33. Read, N. et al. Beyond paired quantum Hall states: parafermions and incompressible states in the first excited Landau level. *Phys. Rev. B* **59**, 8084–8092 (1999).
34. Bonderson, P. et al. Fractional quantum Hall hierarchy and the second Landau level. *Phys. Rev. B* **78**, 125323 (2008).
35. Dolev, M. et al. Dependence of the tunneling quasiparticle charge determined via shot noise measurements on the tunneling barrier and energetics. *Phys. Rev. B* **81**, 161303 (2010).
36. Kane, C. L. et al. Quantized thermal transport in the fractional quantum Hall effect. *Phys. Rev. B* **55**, 15832–15837 (1997).
37. Mross, D. F. et al. Theory of disorder-induced half-integer thermal Hall conductance. Preprint at https://arxiv.org/abs/1711.06278 (2017).
38. Wang, C., Vishwanath, A. & Halperin, B. I. Topological order from disorder and the quantized Hall thermal metal: possible applications to the $\nu = 5/2$ state. Preprint at https://arxiv.org/abs/1711.11557 (2017).
39. Lian, B. et al. Theory of disordered $\nu = 5/2$ quantum thermal Hall state: emergent symmetry and phase diagram. *Phys. Rev. B* **97**, 165124 (2018).
40. Steven, S. H. On the interpretation of thermal conductance of the $\nu = 5/2$ edge. *Phys. Rev. B* **97**, 121406 (2018).

Acknowledgements We acknowledge B. Halperin and S. Simon for discussions. M.B. acknowledges the help and advice of Y. Gross regarding fabrication processes and R. Bhattacharyya for help with the cold amplifiers and Y. C. Chung and H. K. Choi for their help with the dilution refrigerator. M.H. acknowledges the continuous support of the Sub-Micron Center staff, and in particular Y. Rotblat, without whom this work would not be possible. M.H. acknowledges the support of the European Research Council under the European Community's Seventh Framework Program (FP7/2007-2013)/ERC under grant agreement number 339070, the partial support of the Minerva foundation under grant number 711752, the Israeli Science Foundation ISF under grant number 459/16 and, together with V.U., the German Israeli Foundation (GIF) under grant number I-1241-303.10/2014. A.S and Y.O. acknowledge support from the European Research Council under the European Union's Seventh Framework Program (FP7/2007-2013)/ERC Project MUNATOP, the DFG (CRC/Transregi 183, EI 519/7-1) and the Israel Science Foundation. Y.O. acknowledges the Binational Science Foundation (BSF). D.E.F.'s research was supported in part by the National Science Foundation under grant number DMR-1607451.

Reviewer information *Nature* thanks K. Shtengel, S. Simon and the other anonymous reviewer(s) for their contribution to the peer review of this work.

Author contributions M.B. and M.H. designed the experiment, preformed the measurements, did the analysis and guided the experimental work. M.B. fabricated the devices with input from M.H., D.E.F. and Y.O., and A.S. worked on the theoretical aspects. V.U. grew the two-dimensional electron-gas heterostructures. All authors contributed to the write up of the manuscript.

Competing interests The authors declare no competing interests.

Additional information
Extended data is available for this paper at https://doi.org/10.1038/s41586-018-0184-1.
Reprints and permissions information is available at http://www.nature.com/reprints.
Correspondence and requests for materials should be addressed to M.H.
Publisher's note: Springer Nature remains neutral with regard to jurisdictional claims in published maps and institutional affiliations.

© 2018 Macmillan Publishers Limited, part of Springer Nature. All rights reserved.

METHODS

MBE-grown heterostructures. The MBE growth techniques used for heterostructures harbouring the fragile $\nu = 5/2$ fractional state were developed during the past decades. Poor correlation was found between the zero-field mobility and the $\nu = 5/2$ energy gap. The key factor influencing the robustness of the state was found to be the spatial correlations among the charged scatters in the doped layers[29]. The highest quality (largest gap) was observed when using the SPSL scheme accompanied by controlled illumination at low temperatures[41–43]. However, the fabricated devices exhibited poor temporal stability, as well as gate hysteresis[44]. In this work, we used two types of structures, one that had substantial thermal bulk conductance and another that did not (see Extended Data Fig. 1).

Device fabrication. A high-purity heterojunction hosting a high-mobility two-dimensional electron gas, with areal electron density 2.8×10^{11} cm^{-2} and 4.2-K 'dark' mobility $\mu = 20 \times 10^6$ cm^2 V^{-1} s^{-1}, was used. The depth of the two-dimensional electron gas below the surface was 176 nm, the spacer layer (separation between two-dimensional electron gas and donors) was 85 nm and the quantum-well width was 30 nm. A 5-nm-thick HfO_2 layer was deposited on the surface using an atomic layer deposition process and served as a dielectric layer under the gates. Because the crystal direction is found to affect the contact resistance[44,45], 'zigzag edge'-type contacts were fabricated. Etched groves under the floating contact (not visible in the SEM micrograph) ensure that the incident current enters the bulk of the metal ohmic contact before splitting between the different arms of the device. Following a thorough cleaning of the surface (by plasma ashing and oxide removal), contacts were evaporated in an electron-gun evaporator with a base pressure of 10^{-8} torr. The evaporation sequence for ohmic contacts, from the GaAs surface and up, was: Ni (5 nm), Au (200 nm), Ge (100 nm), Ni (75 nm) and Au (15 nm). Contacts were alloyed at 450 °C for 2 min. The continuous gates were evaporated on HfO_2 in the sequence Ti (5 nm) and Au (20 nm).

Continuous gates versus quantum point contact constrictions. Because the heterostructures are doped using the SPSL method[29], 'relatively free' electrons exist in the donor layer. Depleting, or pinching, electrons in the two-dimensional electron gas by using a quantum point contact (QPC) constriction requires a large negative gate voltage of about −10 V (in order to deplete also the donor layer). This leads to considerable hysteresis and instability, presumably due to the 'slow' motion of the carriers in the donor layers. By replacing the QPCs with continuous gates, deposited on a high-dielectric-constant HfO_2 insulator, the required voltage for depletion was about −1 V, thus minimizing the instability and hysteresis effects.

Small floating contact. Owing to the finite contact resistance, backscattering from the floating heated reservoir leads to an effective series thermal resistance and possibly shot noise in the source arm. Backscattering from the contact was measured by comparing the incident current to the reflected one when the number of the fully open arms was changed. The source current was initially fully reflected into the amplifier, thus measuring the impinging current, I_s. Then, in a two-arm configuration, the reflected current, I_{ref}, was measured again. The reflection coefficient r was calculated from $r = 2I_{ref}/I_s - 1$. Similar expressions are used for any N open arms. The measured reflection depended on the cycling round and the filling factor and was always less than 3%.

Branching of current into *N* arms. Because the small floating contact might not have the same contact resistance in each of the four arms, and the density in each arm may be slightly different, the equal branching of the currents in each arm must be verified. Optimization was performed by a changing slightly the magnetic field (Extended Data Fig. 4).

Calibration of the gain and T_0. Knowing the gain of the amplification chain is crucial for the determination of the electron temperature, T_m. Two calibration regions (for the two amplification chains), each composed of an additional gated region and two contacts (source and ground) were added in two opposite arms[26]. Two methods were used to calibrate the gain: (a) verifying the well known quasiparticle charge at a known temperature and (b) measuring thermal noise when the electron temperature was equal to the fridge temperature (at temperatures higher than 70–100 mK). The different effective gains (at 30 kHz bandwidth) were determined at different filling factors by comparing the areas under the resonance curves.

For example, calibrating the gain (of the amplification chain, composed of two amplifiers and a spectrum analyser) via shot-noise measurements proceeded as follows. First, the temperature was determined, independently of the gain, by a linear extrapolation of the noise curve versus the current I (at $eV_s \gg 2k_BT_0$) to zero noise. The intersection point is $eV_s = 2k_BT_0$, with $V_s = Ih/(\nu e^2)$ being the Hall voltage (see Extended Data Fig. 5b and ref. [26]). With the transmission coefficient of the QPC, t_{QPC}, and the known quasiparticle charge, e^*, the gain is determined by a simple matching procedure of the shot noise data with the familiar expression of the spectral density of the noise. We use the usual expression of shot noise for independent scattering events, $S_i = 2e^*It_{QPC}(1 - t_{QPC})\zeta(V, T)$, where $\zeta(V, T)$ is a temperature-dependent factor that has been proven to work quite well in all the quantum Hall effect regimes and V is the applied voltage. T_0 is determined with an accuracy of ±0.5 mK.

The gain is actually an 'effective gain' that depends on the bandwidth of the LCR_H circuit, with $R_H = 1/G_H$, and the spectrum analyser bandwidth. The gain squared is proportional to the area under the Lorentzian power response. Hence, the ratio of these areas at different filling factors should equal the ratio of the squares of the gains. This method was compared with measurements of the thermal noise at elevated temperatures.

It is difficult to determine the systematic errors in the determination of the gain. However, we checked the effect of a slight modification of the gain on the determined temperature T_m and found it to be negligible in comparison with the scattering of the random errors seen in the figures. Interestingly, a correct determination of T_0 led to an extremely good functional fit of the power dissipation with $T_m^2 - T_0^2$ for any number N of open arms and filling factors.

Determining T_m. In a general case of multiple one-dimensional edge modes in each of the N arms, the expressions for the dissipated power and the noise are cumbersome. We express the dissipated power in the floating contact as

$$\Delta P = \frac{1}{2}\frac{I_s^2}{G_H}\frac{\nu_{QPC1}}{\nu^2}\left[1 - \frac{\nu_{QPC1}}{\sum_{i=1}^{i=4}\nu_{QPCi}}\right]$$

where ν_{QPCi} is the filling factor in the QPC. In turn, the temperature T_m is related to the thermal noise via $S_{th} = 2G^*k_B(T_m - T_0)$, with

$$\frac{1}{G^*} = \frac{1}{G_{amp}} + \frac{1}{\sum_{i=1, i\neq amp}^{i=4} G_i}$$

where G_i is the conductance of the ith arm[23–26] and G_{amp} is the conductance of the arm that hosts the amplifier.

Thermal conductance at low temperatures. Here we discuss the observed increase in the thermal conductance at 12 mK at the $\nu = 5/2$ state that is due to the lack of equilibration between the upstream and downstream modes. We show that this behaviour is compatible with the particle–hole Pfaffian model. We argue that because the particle–hole Pfaffian model has only one upstream Majorana mode, the equilibration length $\xi(T)$ is especially long compared to all other quantum Hall states at the lowest temperatures. Thus, the upstream and downstream modes in the particle–hole Pfaffian state may require a higher temperature for equilibration compared to other topological liquids. In what follows, we only focus on the energy exchange between the upstream and downstream modes and do not address how local quasi-equilibrium is established in each mode. We also neglect tunnelling from the fractional channel to the integer ones. We believe that this is justified by the width of the confining potential of the etch-defined edge[46] and by spin conservation.

At the $\nu = 2/3$ state, the thermal conductances of upstream and downstream modes are equal. This leads to a relatively slow temperature dependence of the observed conductances as $K \approx \xi(T)/L$, where L is the edge length and $\xi(T)$ is the equilibration length[26]. A zero thermal conductance is expected only at an infinite L. The exact dependence of $\xi(T)$ on the temperature is determined by the system details but we expect that $\xi(T)$ grows at low temperatures, in agreement with the data. At filling factors such as $\nu = 3/5$, the total thermal conductances of upstream and downstream modes differ. Then, the correction to the universal heat conductance varies as $\exp[-CL/\xi(T)]$, where C is a constant[26]. Thus, only small corrections to the universal value are expected as long as $\xi(T) \ll L$. When $\xi(T) \geq L$, the thermal conductance should grow with decreasing temperature. Such growth has been seen experimentally only at $\nu = 5/2$ and $T < 15$ mK. This suggests that the inequality $\xi(T) \ll L$ holds at accessible temperatures for all states except $\nu = 5/2$ (ref. [36]).

The different behaviour of $\xi(T)$ for different filling factors may originate from the structure of the most relevant inter-mode interaction. In Abelian states this interaction is $\nu(x)\partial_x\phi_i\partial_x\phi_j$, where ϕ_k denotes the kth Bose mode and the interaction amplitude $\nu(x)$ is a random function of coordinates. A state with at least two upstream Majorana modes ε_i exhibits the same scaling of the equilibration length because of the same scaling dimension of the leading inter-mode interaction $\nu(x)\varepsilon_i\varepsilon_j\partial_x\phi_k$. In the particle–hole Pfaffian model, there is only a single upstream Majorana mode ε, and therefore such a term cannot exist in the Hamiltonian. Thus, the interaction is less relevant in the renormalization group sense. This translates into a weaker thermal exchange at low temperatures and a faster growth of the equilibration length at low T.

41. Willett, R. L. The quantum Hall effect at 5/2 filling factor. *Rep. Prog. Phys.* **76**, 076501 (2013).
42. Samani, M. et al. Low-temperature illumination and annealing of ultrahigh quality quantum wells. *Phys. Rev. B* **90**, 121405 (2014).
43. Rössler, C. et al. Gating of high-mobility two-dimensional electron gases in GaAs/AlGaAs heterostructures. *New J. Phys.* **12**, 043007 (2010).
44. Slobodeniuk, A. O. et al. Equilibration of quantum Hall edge states by an Ohmic contact. *Phys. Rev. B* **88**, 165307 (2013).
45. Dahlem, F. Cryogenic scanning force microscopy of quantum Hall samples: adiabatic transport originating in anisotropic depletion at contact interfaces. *Phys. Rev. B* **82**, 121305 (2010).
46. Gelfand, B. Y. et al. Edge electrostatics and a mesa-etched sample and edge-state-to-bulk scattering rate in the fractional quantum Hall regime. *Phys. Rev. B* **49**, 1862–1866 (1994).

© 2018 Macmillan Publishers Limited, part of Springer Nature. All rights reserved.

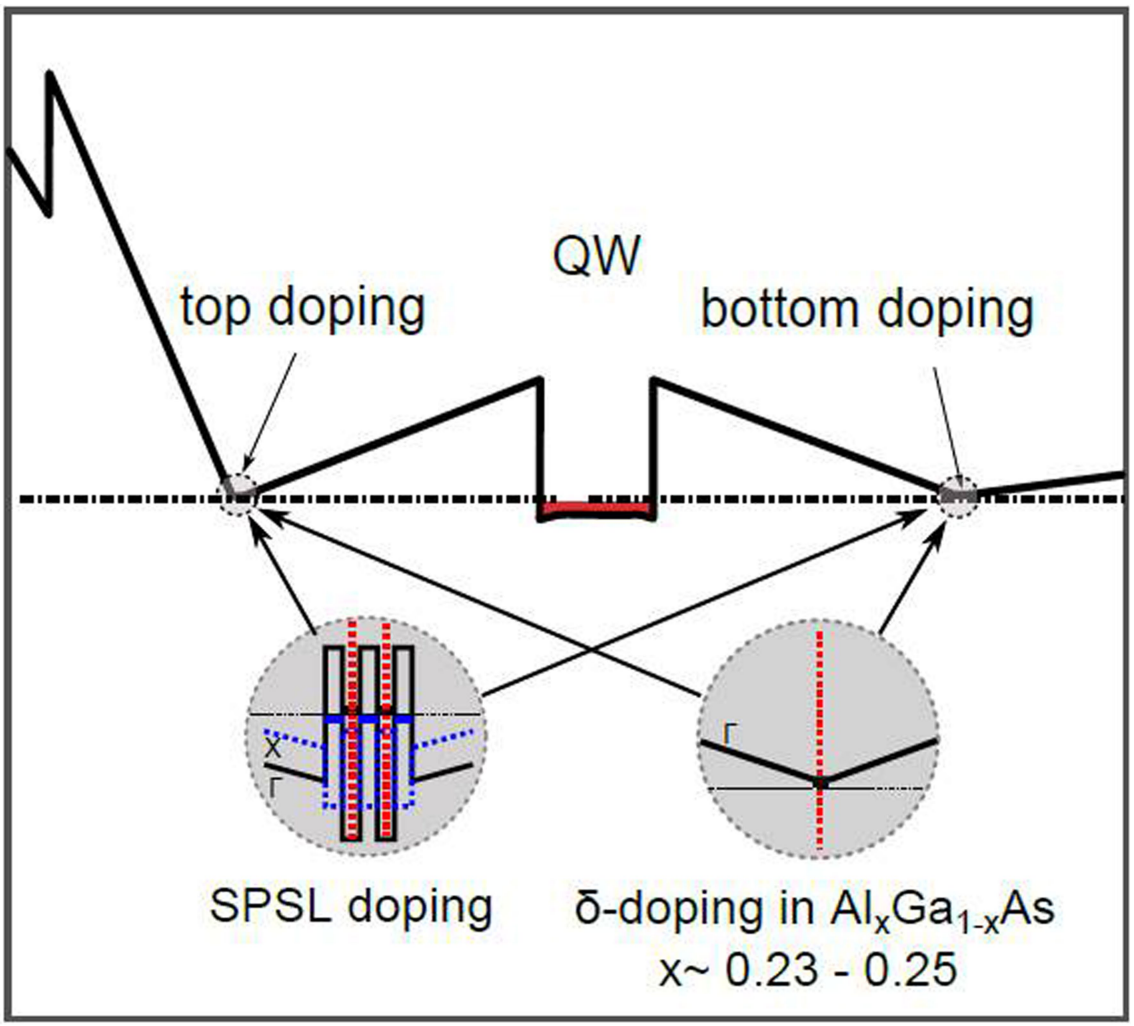

Extended Data Fig. 1 | Details of the growth structure. Schematic of the conduction band in the MBE-grown structures that were studied. The SPSL doping scheme comprises δ–Si doping planes placed in narrow GaAs quantum wells (QW). The thickness of the GaAs and AlAs quantum wells in SPSL is chosen in such a way that the X-band minima of the AlAs layers reside below the Γ-band minimum of the GaAs. Electrons that spill over to the AlAs wells have low mobility and thus do not participate effectively in the conduction process. This structure suffers from substantial added bulk heat conductance. The structure used in our study, with δ–Si doping in low-Al-mole-fraction AlGaAs, did not have a visible bulk thermal conductance.

© 2018 Macmillan Publishers Limited, part of Springer Nature. All rights reserved.

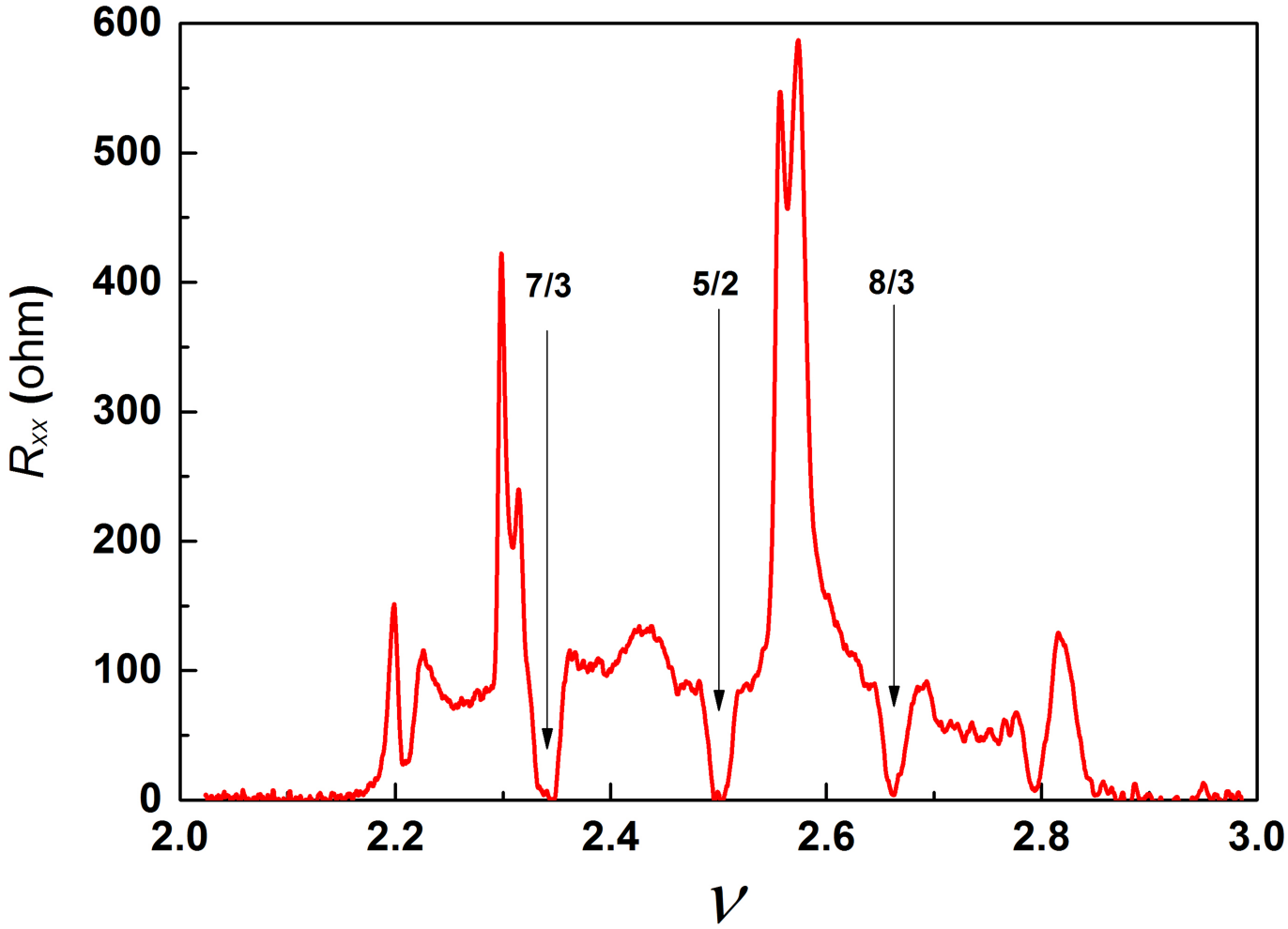

Extended Data Fig. 2 | Longitudinal resistance of the high-mobility SPSL-grown heterostructure. Longitudinal resistance measured in a Hall bar 100 μm wide and 200 μm long. Fractional filling factors are more pronounced than in the δ–Si-doped structure. Yet, the structure suffers from added thermal conductance in the bulk (see main text).

© 2018 Macmillan Publishers Limited, part of Springer Nature. All rights reserved.

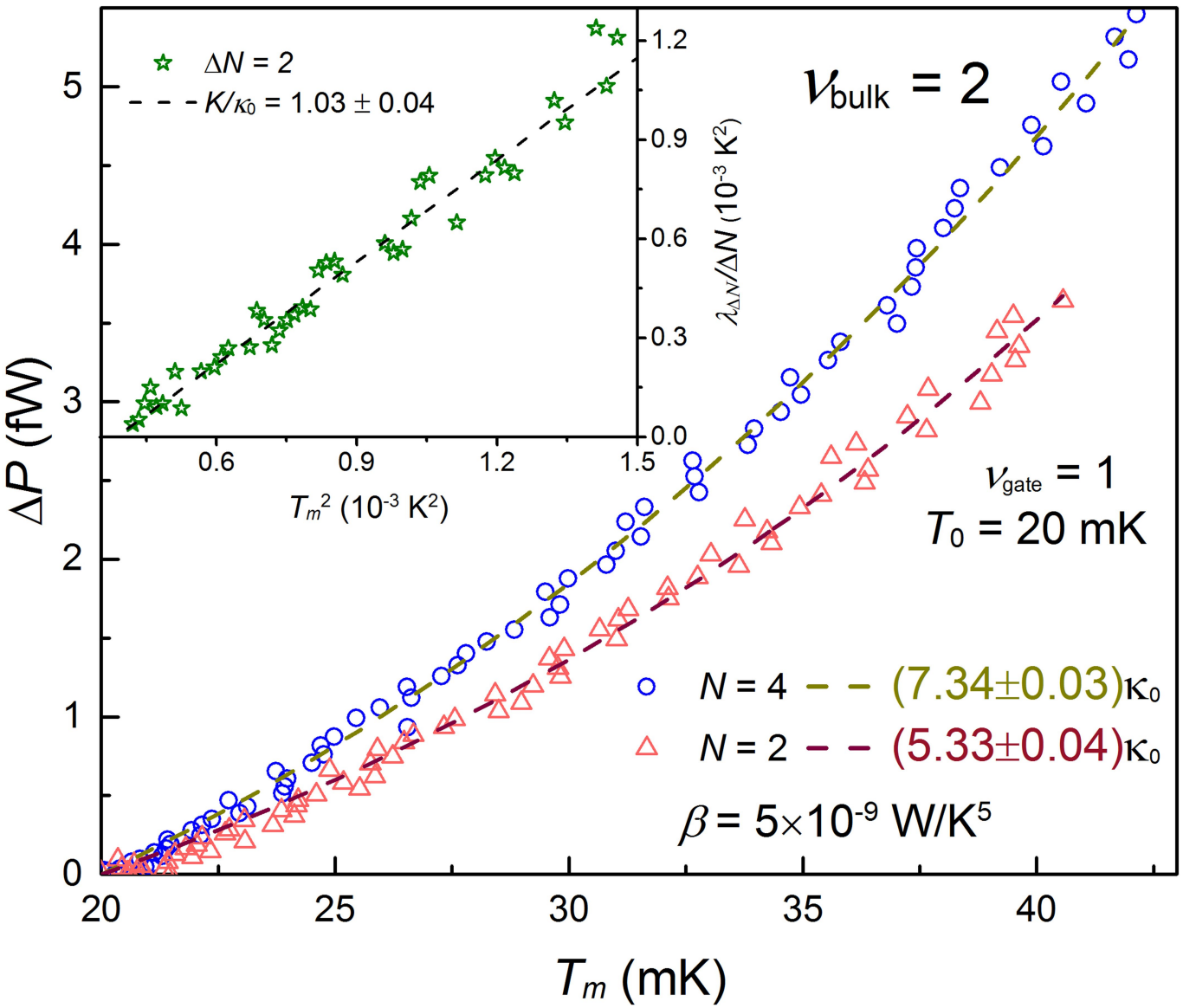

Extended Data Fig. 3 | Thermal noise analysis at $\nu = 2$ in the bulk in the high-mobility SPSL structure. Dissipated power in the floating reservoir is plotted as a function of T_m for different numbers of open arms, N, with one edge mode allowed to flow in each arm (controlled by the surface gates). Dashed curves show the one-parameter fit of α from $\Delta P(\alpha\kappa_0 T^2, \beta T^5)$ for a given β (the value deduced from all the experiments). The apparent total thermal conductance is $K = 7.34\kappa_0$ at $N = 4$ instead of $K = 4\kappa_0$, and $K = 5.33\kappa_0$ at $N = 2$ instead of $K = 2\kappa_0$. The inset shows the dissipated power obtained when subtracting the contributions of a different number of open arms; this cancels the added phonons and bulk contributions, both of which depend only on T_m. The fit line leads to the average thermal conductance per channel $g_Q = (1.03 \pm 0.04)\kappa_0 T$, which agrees with the expectations. (Errors mentioned here correspond to a confidence level of better than 95%.) This device was not used in the experiments.

© 2018 Macmillan Publishers Limited, part of Springer Nature. All rights reserved.

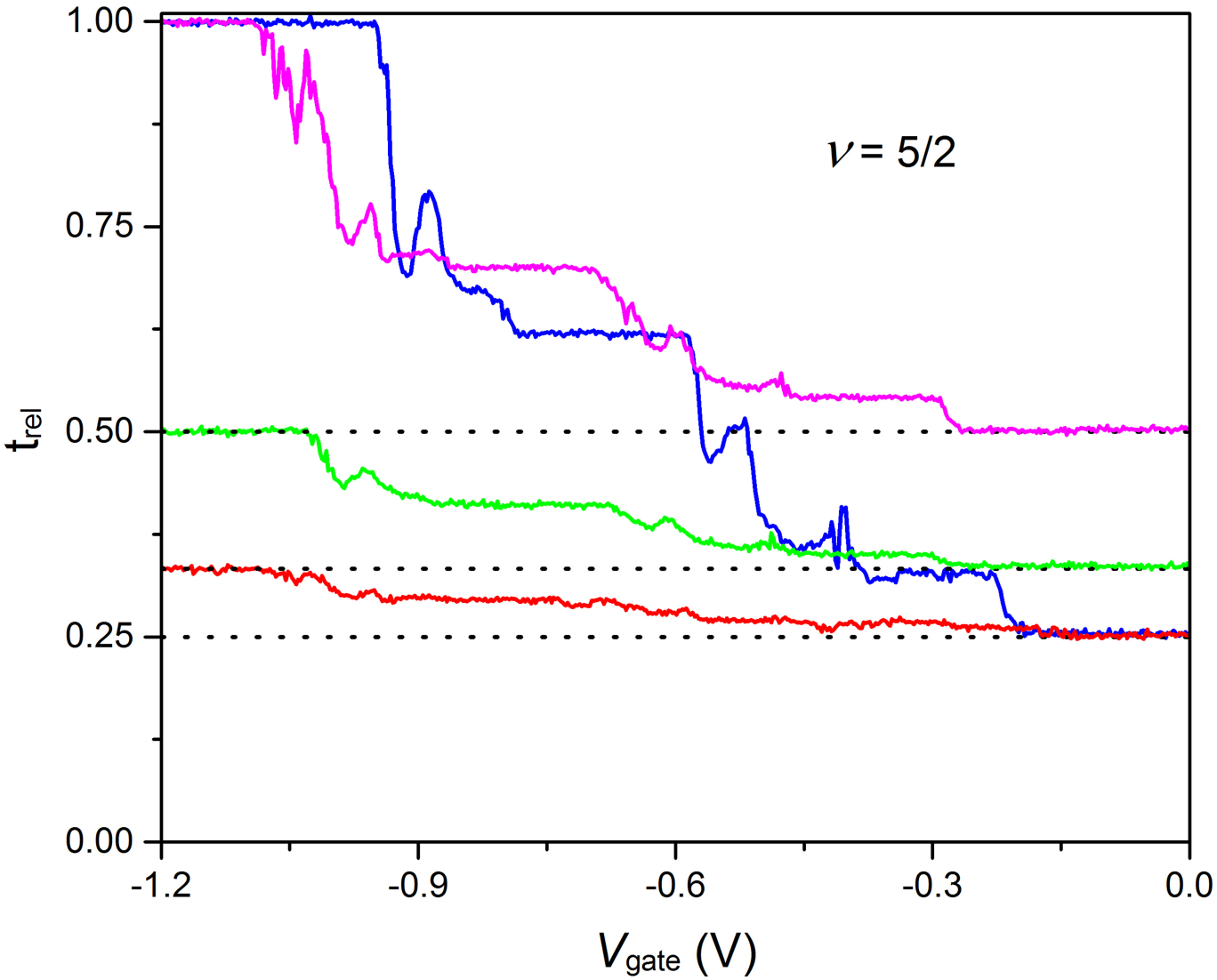

Extended Data Fig. 4 | Equal branching of current in all arms at $\nu = 5/2$. Current is sourced from the source, S, and measured in the drain, D, in the same arm (see Fig. 1a). The blue curve shows the reflection coefficient of the current measured in the drain as a function of the pinching of the arm gate. The reflection coefficient value starts from 0.25, when all the arm gates are fully open, and reaches 1.00, when all the current is reflected. The red, green and magenta curves correspond to measurements for the fully open 'measurement arm', performed while the other arm gates deplete gradually one by one. Four open arms give a reflection coefficient of $r = 0.25$, whereas three open arms lead to $r = 0.33$ and two open arms give $r = 0.50$. The dotted lines are guides for the eyes indicating equal branching of currents.

© 2018 Macmillan Publishers Limited, part of Springer Nature. All rights reserved.

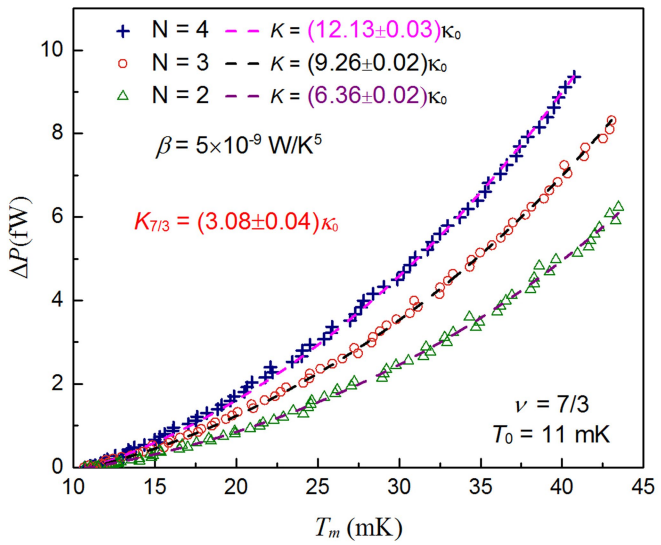

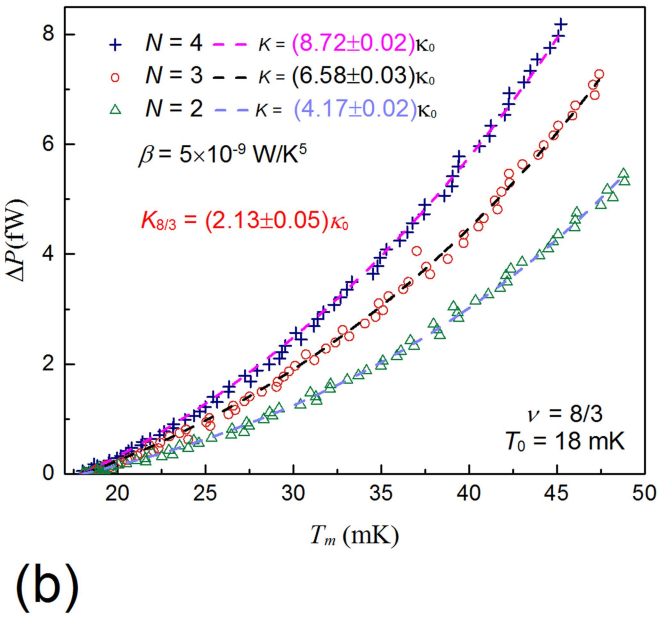

Extended Data Fig. 5 | Thermal noise analysis at $\nu = 7/3$ and $\nu = 8/3$. **a**, **b**, Standard analysis (see main text), without subtracting the number of participating arms, but using the phonon contribution coefficient β, which fits extremely well in a large range of temperatures and at different filling factors (errors of the fit are 99% confidence levels). The agreement with the expected data is clear. We note the added thermal heat conductance at $\nu = 8/3$ (**b**; see text).

© 2018 Macmillan Publishers Limited, part of Springer Nature. All rights reserved.

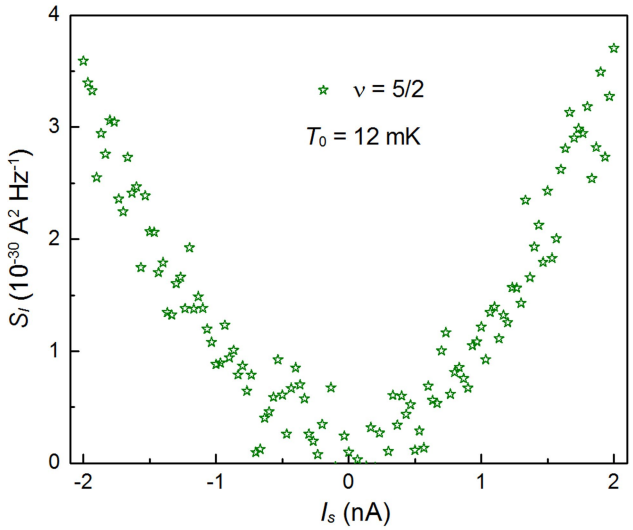

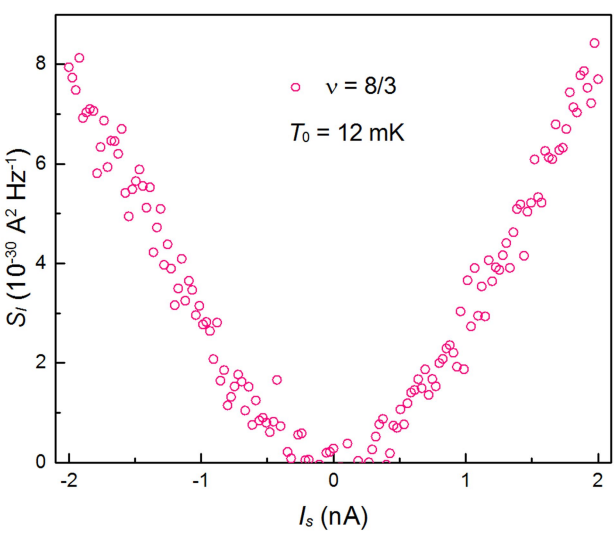

Extended Data Fig. 6 | Upstream neutral modes in $\nu = 5/2$ and $\nu = 8/3$. **a**, **b**, The noise measured at an upstream floating contact connected to the cold amplifier (with respect to ground) is clear evidence of upstream neutral modes. Such upstream noise is not found in particle-like states[21].

© 2018 Macmillan Publishers Limited, part of Springer Nature. All rights reserved.